

FULLY COUPLED STRUCTURAL-UNSTEADY AERODYNAMICS MODELLING FOR AEROELASTIC RESPONSE OF ROTORCRAFT

G. Bernardini, J. Serafini, M. Molica Colella, M. Gennaretti

University Roma Tre
Dept. of Mechanical and Industrial Engineering
Via della Vasca Navale 79 - 00146 Rome, Italy
e-mail: g.bernardini@uniroma3.it

ABSTRACT

This paper deals with a computational aeroelastic tool for the analysis of rotorcraft. It has been developed by coupling a nonlinear beam model for blades (and wing) structural dynamics description with a boundary integral equation solver for the prediction of aerodynamic loads. This solver is based on three-dimensional, unsteady, potential aerodynamic formulation. The Galerkin method is used for the spatial integration, whereas the periodic blade (and wing) response is determined by a harmonic balance approach. This aeroelastic model yields a unified approach for aeroelastic response and blade pressure prediction that may conveniently be used for aeroacoustic purposes and, in addition, is able to examine configurations where blade-vortex interactions and multiple-body aerodynamic interactions occur. Numerical results show the capability of the aeroelastic tool to evaluate blade response and vibratory hub loads for a helicopter main rotor in level flight conditions, and examine the efficiency and robustness of the different computational algorithms that might be applied in the presented aeroelastic solver. A sensitivity analysis of the predictions on the aerodynamics model used will be also discussed.

INTRODUCTION

The aim of this work is to present some features and recent advances of a computational tool for the analysis of the aeroelastic response of helicopters and tiltrotors. Rotorcraft are affected by strong couplings between elastic deformations and aerodynamic loads, which significantly contribute to the vibrations transmitted to the fuselage, as well as, to the emitted noise. A great variety of flight conditions may be experienced by rotary-wing aircraft, each yielding specific aerodynamic environment and corresponding elastic response. For instance, in the descent flights of helicopters strong BVI (Blade-Vortex Interaction) characterizes both vibrations and noise levels, while for tiltrotors in airplane mode the impact of

prop rotor wake on the wing is a major contribution to vibrations which requires an accurate simulation for providing a reliable aeroelastic response.

The computational aeroelastic tool for rotary-wing aircraft presented is the result of the research work done by the authors during the last years [1]. It uses a three-dimensional, unsteady, aerodynamic solver based on the Boundary Element Method (BEM) for potential flows introduced in Ref. [2] as a development of the formulation presented in Ref. [3], that is able to predict strong BVI effects, with inclusion of the wake-wing impacts arising on tiltrotor configurations. This solver can be applied both for direct evaluation of the aerodynamic loads and for the calculation of the wake inflow to be used within a section-load aerodynamic model. The structural model for the helicopter rotor blades (and wing-prop rotor systems, as well) is based on the beam theory developed in Ref. [4]. It consists of a nonlinear bending-torsional model (with inclusion of the gimbal equations, if it is present). The resulting set of integro-differential equations is discretized spatially through the Galerkin approach based on the natural modes of vibration of a cantilever, nonrotating beam (with additional rigid-body modes, if necessary). The aerodynamic and the structural solvers are fully coupled by forcing the structural equations with the aerodynamic generalized loads computed by the BEM approach and evaluating the aerodynamic boundary conditions from the deformations given by the structural model. Considering arbitrary steady flight conditions, the aeroelastic responses given in terms of blade deflections and vibratory loads (in rotating and nonrotating frames) are obtained through a harmonic balance procedure that iteratively updates periodic deformations and aerodynamic loads until convergence. When the aerodynamic solver is applied for the direct evaluation of loads (fully-coupled mode solution), the blade pressure distribution is among the outputs of the solution procedure which, in turn, may be applied in aeroacoustic formulations for the identification of the noise field emitted.

Aerodynamic and structural models, as well as the techniques applied for the numerical integration of the fully coupled aeroelastic system will be described with details in the following. In addition, a numerical investigation of the efficiency and robustness of different computational algorithms that might be applied in the fully-coupled mode aeroelastic solution will be examined, along with the sensitivity of the predictions on the aerodynamic model used.

STRUCTURAL DYNAMICS MODELLING

Beam-like models are applied to describe the structural dynamics of helicopter rotor blades, as well as that of wing and proprotor blades of tiltrotors. These are based on the nonlinear bending-torsion formulation presented in Ref. [4], that is valid for straight, slender, homogeneous, isotropic, nonuniform, twisted blades, undergoing moderate displacements.

For rotor blade analysis, second order terms are retained in the equations after application of an ordering scheme dropping third-order terms (with respect to bending slope) not contributing to damping. The radial displacement is eliminated from the set of equations by solving it in terms of local tension, and thus the resulting structural operator consists of a set of coupled nonlinear differential equations governing the bending of the elastic axis and the blade torsion [5]. If present, the effects of blade precone angle, hinge offset, torque offset and mass offset are included in the model.

For tiltrotor analysis, the interactions between wing and propellers are such that the wing deformation affects proprotor blades kinetics and, in turn, proprotor hub loads force wing dynamics [6].

AERODYNAMICS MODELLING

The aerodynamics of helicopters is significantly affected by the interactions among main rotor, fuselage and tail rotor, as well as the aerodynamics of tiltrotors is significantly affected by the interactions between proprotors and wing. In particular, a crucial role is played by the interactions between bodies and wakes (body-wake interactions, BVI). These include blade-wake and wing-wake impacts that produce impulsive pressures on the body surfaces, and then strongly contribute to the vibratory loads transmitted to the airframe and generate extremely annoying acoustic effects. Therefore, a simulation tool applied for the optimal design of new generation helicopters and tiltrotors has to be able to predict BVI occurrence and corresponding aeroelastic and aeroacoustic effects. In view of this, a boundary integral formulation for potential flows suited for the prediction of strong aerodynamic interaction effects has been presented in Ref. [2]. It is a development of the formulation introduced in Ref. [3] and further extended to rotors in forward flight in Ref. [7]. A brief outline of the potential-flow formulation suited for BVI analysis is given in the following.

It introduces the decomposition of the potential field into an incident field, φ_I , and a scattered field, φ_S . The

scattered potential is generated by sources and doublets over the body surfaces, S_B , and by doublets over the wake portion that is very close to the trailing edge from which emanated (near wake, S_W^N). The incident potential is generated by the doublets over the complementary wake region that compose the far wake, S_W^F . This is the wake portion that may come in contact with other blades. The scattered potential is discontinuous across S_W^N , whereas the incident potential is discontinuous across S_W^F . Hence, as demonstrated in Ref. [2], for $\varphi = \varphi_I + \varphi_S$ the scattered potential is obtained by

$$\begin{aligned} \varphi_S(\mathbf{x}, t) &= \int_{S_B} \left[G(\chi - \chi_I) - \varphi_S \frac{\partial G}{\partial n} \right] dS(\mathbf{y}) \\ &\quad - \int_{S_W^N} \Delta\varphi_S \frac{\partial G}{\partial n} dS(\mathbf{y}) \end{aligned} \quad (1)$$

where $G = -1/4\pi r$ is the unit-source solution of the 3D Laplace equation, with $r = \|\mathbf{y} - \mathbf{x}\|$, while $\Delta\varphi_S$ is the potential jump across the wake surface, that is known from the past history of the potential discontinuity at the trailing edge of the corresponding body through the Kutta-Joukowski condition [2]. In addition, $\chi = \mathbf{v} \cdot \mathbf{n}$, with \mathbf{v} representing the body velocity and \mathbf{n} its outward unit normal, whereas $\chi_I = \mathbf{u}_I \cdot \mathbf{n}$, with the velocity induced by the far wake, \mathbf{u}_I , given by

$$\begin{aligned} \mathbf{u}_I(\mathbf{x}, t) &= \nabla\varphi_I(\mathbf{x}, t) \\ &= -\nabla \int_{S_W^F} \Delta\varphi_S(\mathbf{y}_w^{TE}, t - \vartheta) \frac{\partial G}{\partial n} dS(\mathbf{y}) \end{aligned} \quad (2)$$

The incident potential affects the scattered potential through the induced-velocity term, χ_I , and, in turn, the scattered potential affects the incident potential by its trailing-edge discontinuity that is convected along the wake and yields the intensity of the doublet distribution over the far wake.

Obtaining the discrete form of Eq. (2) by using N panels over the far wake and recalling the vortex-doublet equivalence, the incident velocity field may be evaluated through the following expression

$$\mathbf{u}_I(\mathbf{x}, t) \approx -\sum_{k=1}^N \Delta\varphi_S(\mathbf{y}_{w_k}^{TE}, t - \vartheta_k) \int_{C_k} \nabla_{\mathbf{x}} G \times d\mathbf{y} \quad (3)$$

where $\mathbf{y}_{w_k}^{TE}$ is the trailing edge position where the wake material point currently in \mathbf{y}_{w_k} emanated at time $t - \vartheta_k$, C_k denotes the contour line of the k -th far wake panel, and $\nabla_{\mathbf{x}}$ denotes gradient operator with respect to the variable \mathbf{x} . This equation represents the velocity field given by the Biot-Savart law applied to the vortices having the shape of the far wake panel contours and intensity $\Delta\varphi_S(\mathbf{y}_{w_k}^{TE}, t - \vartheta_k)$. Equation (3) is applied to evaluate both the term χ_I in equation (1) and, once extended to the whole wake, the velocity field from which the wake shape evolution is determined (free-wake analysis). Note that for an accurate prediction of BVI phenomena it is usually essential the accurate evaluation of the wake distortion in that a crucial role is played by the relative positions between body and wake.

The final step of the formulation consists of introducing in Eq. (3) a finite-thickness vortex model that assures

a regular distribution of the induced velocity within the vortex core, and thus a stable and regular solution even in body-vortex impact conditions [2].

Equation (1) is solved numerically by boundary elements, *i.e.*, by dividing S_B and S_w^N into quadrilateral panels, assuming φ_S , χ , χ_I and $\Delta\varphi_S$ to be piecewise constant (zero-th order, boundary element method - BEM), and imposing that the equation be satisfied at the center of each body element (collocation method) [2].

Once the potential field is known, the Bernoulli theorem yields the pressure distribution (see Appendix A) and hence blade loads may be evaluated through integration.

Aerodynamic loads from airfoil theories

Akin to the solution procedures applied in several aeroelastic prediction tools commonly used in rotorcraft applications, in the present solver non fully-coupled solutions may be obtained. These are based on the evaluation of the aerodynamic forcing terms obtained as spanwise integration of the loads given by sectional aerodynamics models derived from airfoil unsteady aerodynamics theories, and corrected with wake inflow (from the BEM solver) to take into account three-dimensional effects due to wake vortices.

For a thin, straight airfoil moving in an incompressible flow, following the Greenberg theory [8] (which is the extension of the Theodorsen theory [9] to pulsating airstream) it is possible to determine the aerodynamic force acting on it by combining the non-circulatory lift, L_{nc} , orthogonal to the chord with the circulatory lift, L_c , directed along the normal to the relative wind (see, for instance, Ref. [5]). Specifically, for ρ denoting the air density and b denoting the airfoil semi-chord length, the non-circulatory lift is expressed as

$$L_{nc}(t) = \pi \rho b^2 \dot{v}_{1/2}^n \quad (4)$$

where $\dot{v}_{1/2}^n$ denotes the time derivative of the normal component of the relative wind evaluated at the airfoil mid point (positive upwards). The circulatory lift, that in practical applications is the most relevant load contribution, is given by the following expression

$$L_c(t) = 2 \pi \rho b V \mathcal{F}^{-1} [C(k) \tilde{v}_{3/4}^n] \quad (5)$$

where V denotes the relative wind velocity, \mathcal{F} denotes Fourier transformation and $\tilde{v}_{3/4}^n = \mathcal{F}(v_{3/4}^n)$, with $v_{3/4}^n$ representing the normal component of the relative wind evaluated at the airfoil 3/4-chord point. In addition, $C(k)$ is the lift deficiency (complex) function defined by Theodorsen [9] in terms of the reduced frequency, $k = \omega b / \bar{V}$, where ω is the variable in the Fourier domain and \bar{V} is the mean (or reference) value of V which is responsible for the shed vorticity convection (see Ref. [10] for a detailed analysis of the effects of non-uniform convection of the shed vorticity along the wake). For a harmonic $v_{3/4}^n$ input, $C(k)$ defines gain and phase shift of the L_c/V harmonic response. The set of the aerodynamic loads acting on the airfoil includes also the pitching moment about the 1/4-chord point (positive clockwise for the relative wind directed from left to right),

which is given by [8]

$$M_{1/4}(t) = -\frac{b}{2} L_{nc} - \pi \rho \frac{b^3}{2} \left(V \omega_a + \frac{b}{4} \dot{\omega}_a \right) \quad (6)$$

where ω_a is the angular velocity of the airfoil. Once $v_{1/2}^n$, $v_{3/4}^n$, ω_a and V are expressed in terms of the blade degrees of freedom (a major elastic contribution from blade lag may appear also in V), Eqs. (4), (5) and (6), combined with a model to take into account drag effects, may be applied to develop aeroelastic formulations for wings and rotors.

HARMONIC BALANCE FOR AEROELASTIC RESPONSE ANALYSIS

The equations governing the blade structural dynamics coupled with the unsteady aerodynamic load modelling yield the aeroelastic integro-differential equations to be integrated. Here, the space integration is performed through the Galerkin approach, starting from the description of the elastic axis deformation as a linear combination of shape functions that satisfy homogeneous boundary conditions. The resulting aeroelastic system consists of a set of nonlinear ordinary differential equations of the type

$$\mathbf{M}(t) \ddot{\mathbf{q}} + \mathbf{C}(t) \dot{\mathbf{q}} + \mathbf{K}(t) \mathbf{q} = \mathbf{f}_{str}^{nl}(t, \mathbf{q}) + \mathbf{f}_{aer}(t, \mathbf{q}) \quad (7)$$

where \mathbf{q} denotes the vector of the Lagrangian coordinates, whereas \mathbf{M} , \mathbf{C} , and \mathbf{K} are time-periodic, mass, damping, and stiffness structural matrices representing the linear structural terms (note that these matrices are time-variant because of the cyclic pitch contribution). Nonlinear structural contributions are collected in the forcing vector $\mathbf{f}_{str}^{nl}(t, \mathbf{q})$, whereas vector $\mathbf{f}_{aer}(t, \mathbf{q})$ collects the generalized aerodynamic forces. The aerodynamic loads may be obtained either by integration along blade and wing surfaces of the pressure distribution given by the BEM solver outlined above (fully-coupled solution), or by spanwise integration of the expressions in Eqs. (4)-(6) derived from the airfoil theory, combined with the wake inflow predicted by the BEM solver (non fully-coupled solution).

Since the aim is the prediction of the aeroelastic steady periodic response during forward flight, the aeroelastic system in Eq. 7 is solved by using the harmonic balance approach. It is a methodology suitable for the analysis of the asymptotic solution (as time goes to infinity) of differential equations forced by periodic terms, as in the present case. The harmonic balance solution consists of: (i) express LHS and RHS of the aeroelastic system (Eq. 7) in terms of their Fourier series; (ii) equate the resulting coefficients; (iii) solve the corresponding algebraic system in terms of the unknown Fourier coefficients of the Lagrangian coordinates of the problem. Specifically, expressing \mathbf{q} and $\mathbf{f} = \mathbf{f}_{str}^{nl} + \mathbf{f}_{aer}$ in terms of the following Fourier series

$$\begin{aligned} \mathbf{q}(t) &= \mathbf{q}_0 + \sum_{n=1}^N [\mathbf{q}_n^c \cos(\Omega_n t) + \mathbf{q}_n^s \sin(\Omega_n t)] \\ \mathbf{f}(t) &= \mathbf{f}_0 + \sum_{n=1}^N [\mathbf{f}_n^c \cos(\Omega_n t) + \mathbf{f}_n^s \sin(\Omega_n t)] \end{aligned}$$

(where $\mathbf{q}_n^c, \mathbf{q}_n^s, \mathbf{f}_n^c$ and \mathbf{f}_n^s denote cosine and sine components of the n -th harmonic of \mathbf{q} and \mathbf{f} , whereas $\Omega_n = n\Omega$, with Ω representing the fundamental frequency *i.e.*, the rotor angular velocity) and then combining with Eq. 7 yields the following representation of the aeroelastic system harmonic components

$$\left[\hat{\mathbf{M}} + \hat{\mathbf{C}} + \hat{\mathbf{K}} \right] \hat{\mathbf{q}} = \hat{\mathbf{f}} \quad (8)$$

where

$$\hat{\mathbf{q}}^T = \left\{ \mathbf{q}_0^T \quad \mathbf{q}_1^c{}^T \quad \mathbf{q}_1^s{}^T \quad \mathbf{q}_2^c{}^T \quad \mathbf{q}_2^s{}^T \quad \dots \right\}$$

and

$$\hat{\mathbf{f}}^T = \left\{ \mathbf{f}_0^T \quad \mathbf{f}_1^c{}^T \quad \mathbf{f}_1^s{}^T \quad \mathbf{f}_2^c{}^T \quad \mathbf{f}_2^s{}^T \quad \dots \right\}$$

Matrices $\hat{\mathbf{M}}, \hat{\mathbf{C}}$ and $\hat{\mathbf{K}}$ in Eq. 8 come out from Eq. 7 by combining the harmonics of the $\mathbf{q}, \dot{\mathbf{q}}$ and $\ddot{\mathbf{q}}$ terms with the harmonics of the matrices \mathbf{M}, \mathbf{C} , and \mathbf{K} (see Ref. [1] for details). In particular, if \mathbf{M}, \mathbf{C} , and \mathbf{K} were constant matrices, in Eq. 8 one would have block-diagonal matrices and each harmonic of \mathbf{q} would depend only on the same harmonic of \mathbf{f} (the \mathbf{q} -harmonics equations would be uncoupled). Instead, in the problem under examination the structural matrices are periodic and hence, once expressed in terms of the Fourier series and combined with the harmonics of $\mathbf{q}, \dot{\mathbf{q}}$ and $\ddot{\mathbf{q}}$, they yield fully-populated $\hat{\mathbf{M}}, \hat{\mathbf{C}}$ and $\hat{\mathbf{K}}$ matrices, thus coupling the algebraic equations for the unknown harmonics in $\hat{\mathbf{q}}$.

Because of the presence of nonlinear structural terms and of aerodynamic contributions in $\hat{\mathbf{f}}$, Eq. 8 has to be solved using an iterative procedure. To this aim, the Newton-Raphson method is applied. Specifically, the harmonic aeroelastic solution is obtained from convergence of the following iterative procedure (with n indicating the iteration step number)

$$\hat{\mathbf{q}}_n = \left[\hat{\mathbf{M}} + \hat{\mathbf{C}} + \hat{\mathbf{K}} - \hat{\mathbf{J}}_{n-1}^{aer} \right]^{-1} \left[\hat{\mathbf{f}}_{n-1} - \hat{\mathbf{J}}_{n-1}^{aer} \hat{\mathbf{q}}_{n-1} \right] \quad (9)$$

where $\hat{\mathbf{J}}_{n-1}^{aer}$ is the aerodynamic Jacobian evaluated at $\hat{\mathbf{q}} = \hat{\mathbf{q}}_{n-1}$, while $\hat{\mathbf{f}}_{n-1}$ denotes the sum of nonlinear structural terms and aerodynamic loads evaluated at $\hat{\mathbf{q}} = \hat{\mathbf{q}}_{n-1}$ (*i.e.*, through the Lagrangian coordinates given by the previous iteration step). Under this assumption, the aerodynamic portion of the forcing term is equivalent to $\hat{\mathbf{f}}_0^{aer} + \hat{\mathbf{f}}_{aer}^{nl}$, with $\hat{\mathbf{f}}_0^{aer}$ denoting the aerodynamic load portion that is not influenced by the structural deformation. For the sake of computational time saving, the approximation of maintaining constant the aerodynamic Jacobian might be applied (indeed, this would avoid the evaluation of the inversion of the global Jacobian matrix at each step of the iterative process).

Evaluation of aerodynamic Jacobian

The aerodynamic Jacobian is evaluated numerically. Observing that, at a given iteration step, it relates the harmonics of each perturbation structural Lagrangian variable to the harmonics of the corresponding generalized aerodynamic forces, it is identified through a sequence of time-marching harmonic responses of the BEM solver. Specifically, for a given Lagrangian variable, the perturbation harmonic responses to each of the $2N + 1$ (small

amplitude) perturbation Fourier components considered are evaluated. The (input and output) perturbations are defined about the Fourier components corresponding to the previous step solution. The Fourier components of each (multi-harmonic) set of output perturbation forces divided by the corresponding input perturbation yield one column of the aerodynamic Jacobian matrix to be used in Eq. 9, *i.e.*:

$$\hat{\mathbf{J}}_{ij}^{aer} = \frac{\hat{f}_i^{aer}(\hat{q}_j + \Delta\hat{q}_j) - \hat{f}_i^{aer}(\hat{q}_j)}{\Delta\hat{q}_j} \quad (10)$$

NUMERICAL RESULTS

Here, some results from the aeroelastic formulation outlined above are presented, with the aim of assessing the efficiency and robustness of different computational algorithms that might be used in the fully-coupled aeroelastic tool, along with analyzing the sensitivity of the aeroelastic response (blade tip deflections and vibratory hub loads) on the used aerodynamic mode.

For these analyses, the four-bladed rotor examined in Ref. [12], at which the reader is referred to for details about structural and inertia properties, is considered. It has radius $R = 4.93\text{m}$, constant chord $c = 0.395\text{m}$, NACA 0012 section profile and a linear twist angle of -8° . The rotor has been examined in level flight conditions with rotational speed $\Omega = 40\text{rad/s}$, at advance ratios $\mu = 0.15$ and $\mu = 0.3$. For the two advance ratios investigated, shaft angle and blade collective and cyclic pitch control angles are those determined in Ref. [12] with linear inflow.

Advance Ratio $\mu = 0.30$

First, a convergence analysis of the iterative aeroelastic solution algorithm is presented in Fig.1. Specifically,

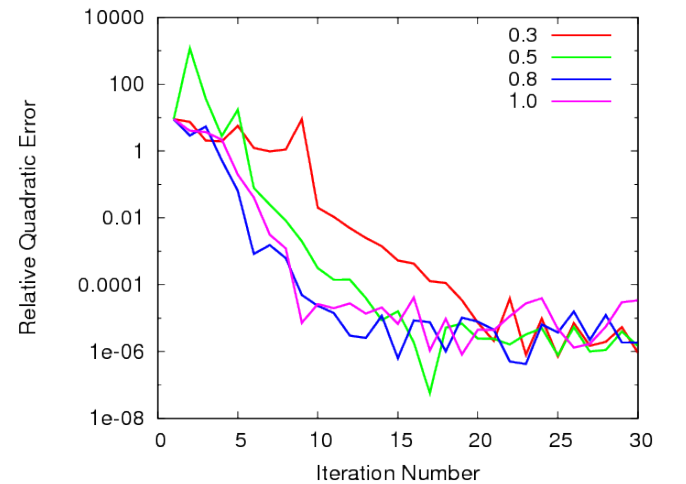


Figure 1. Effect of relaxation factor on convergence history. $\mu = 0.3$.

it shows the effect of the relaxation factor used in the Newton-Raphson method in the error decay (note that here the relaxation factor is defined as a coefficient that multiplies the vector $\hat{\mathbf{f}}_{n-1}$ in Eq. 9). The relative quadratic error is evaluated in terms of the difference between the

vibratory hub loads computed at two iteration steps. This choice is motivated by the fact that from the practical point of view the interesting outcomes of the aeroelastic response analysis are vibratory hub loads and blade deflections, and that the convergence of the former implies the convergence of the latter. For computational time saving, the aerodynamic Jacobian is kept constant during the iterative process (thus yielding the so-called fixed slope iteration procedure), equal to that evaluated numerically about the undeformed configuration ($\mathbf{q} = \mathbf{0}$). The solution histories show that this approach is effective and leads to solution convergence for any value of the relaxation factor, although a relaxation factor close to 1 seems to increase slightly the convergence speed.

In addition, note that a similar convergence history has been achieved by using the constant aerodynamic Jacobian evaluated about the aeroelastic solution predicted by a simpler model based in quasi-steady aerodynamics (this means that the aerodynamic Jacobian is not subject to significant variations in the neighborhood of the state $\mathbf{q} = \mathbf{0}$, and thus the most convenient procedure of evaluating it about the undeformed configuration seems to be appropriate).

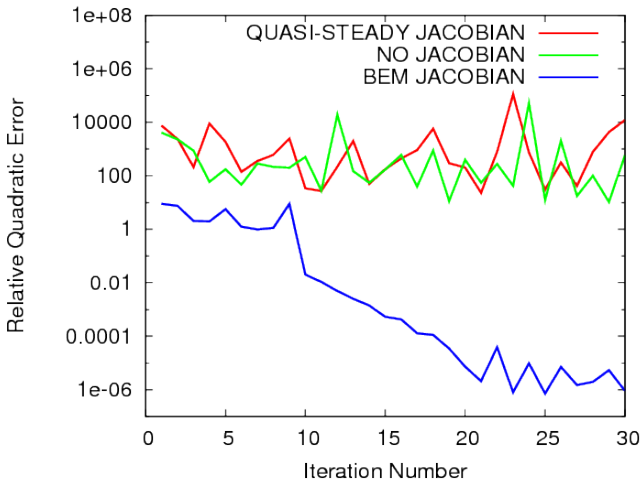


Figure 2. Effect of aerodynamic Jacobian modelling on convergence history. $\mu = 0.3$.

Next, Fig. 2 shows the effect of the use of aerodynamic Jacobian from different aerodynamic models on convergence. Specifically, the results obtained by using the Jacobian evaluated through the BEM solver are compared with those obtained by using the Jacobian evaluated through the quasi-steady aerodynamics, as well as with those determined from the elimination of the aerodynamic Jacobian. As expected, no convergence is achieved when the aerodynamic Jacobian is not included in the solution algorithm, but it is interesting to observe that a very similar negative result is obtained when the Jacobian from the quasi-steady aerodynamic model is applied. This suggests the necessity of using the same aerodynamic solver for solution and Jacobian evaluation.

Then, in order to examine the possibility of reducing the computational costs, a further survey was conducted on the impact of the BEM mesh used for the evaluation of the Jacobian matrix on the solution convergence (in-

deed, as explained above, the numerical identification of the aerodynamic Jacobian might require the evaluation of a high number of aeroelastic responses, thus resulting too computationally expensive). Three different meshes have been considered, as given in Table 1 (note that ‘Solution’ mesh indicates the mesh applied also for the evaluation of the aerodynamic loads forcing the aeroelastic equations).

	N_B	N_W	N_T	Time Step [s]	Calculation Time [min]
Coarse	192	720	1	0.0031	4
Finer	384	1920	2	0.0017	15
Solution	1536	8640	3	0.0011	200

Table 1. BEM mesh and solution data for Jacobian evaluation. N_B =body panels, N_W =wake panels, N_T =wake turns.

The results of this analysis are depicted in Fig. 3 that demonstrates that the application of a very high fidelity (and computationally expensive, see Table 1) Jacobian does not yield a convergence rate significantly faster than those provided by the use of less accurate (and less computationally expensive) Jacobians. Indeed, even the solution from a coarse (and computationally cheap) mesh for Jacobian evaluation is acceptable.

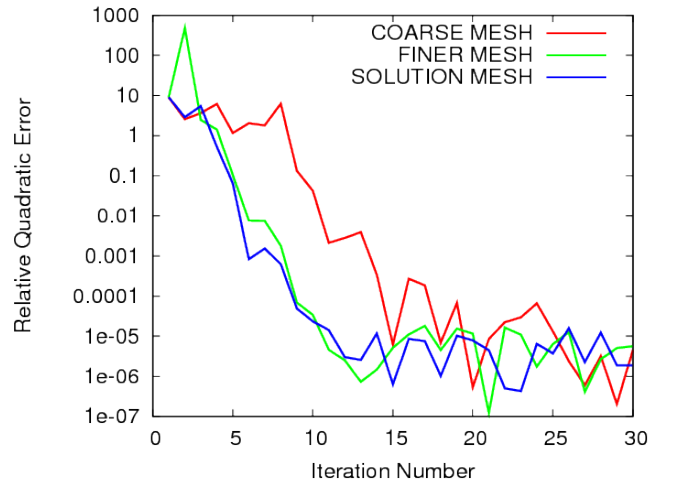


Figure 3. Effect of BEM mesh used for Jacobian evaluation on convergence history. $\mu = 0.3$.

Finally aeroelastic response obtained by using the proposed fully-coupled aeroelastic model is compared with that obtained through the application of a quasi-steady aerodynamic model in the solution procedure. The results are given in terms of blade tip displacements (Fig. 4) and vibratory hub loads (Figs. 5). As flap and lag time histories show a similar behaviour, torsion from the BEM aerodynamic solution presents a higher harmonic content, probably due to the more accurate evaluation of the wake inflow that plays a significant role on this class of problems. Similar considerations can be made about the evaluated $4/rev$ vibratory hub loads, for which the most relevant differences between the two aeroelastic solutions appear in the out-of-plane loads, F_z and M_z , that are more directly related to the blade elastic torsion deformation.

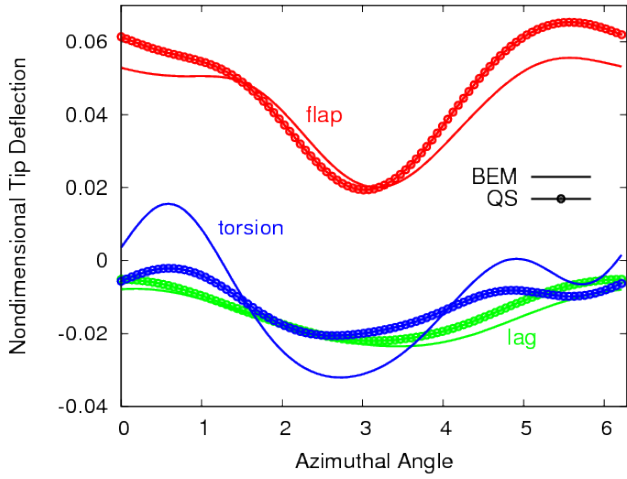


Figure 4. Blade tip deflections. $\mu = 0.3$.

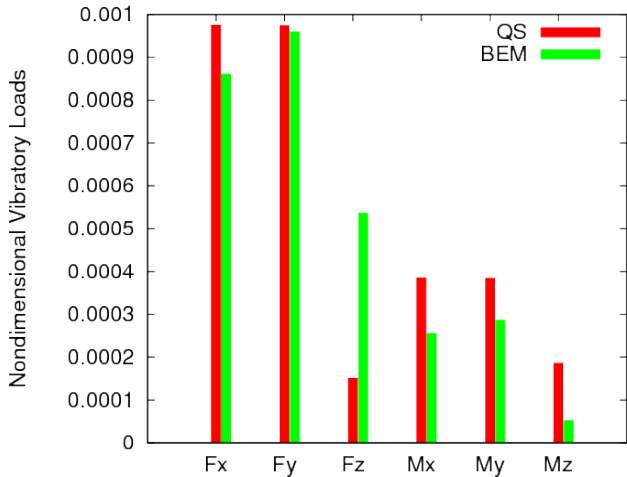


Figure 5. $4/rev$ vibratory hub loads. $\mu = 0.3$.

Advance Ratio $\mu = 0.15$

Next, the above analyses have been repeated for a rotor flight at lower advance ratio. In this condition the strong influence of the velocity field induced by the wake remaining closer to the rotor disk might negatively affect the convergence of the numerical scheme.

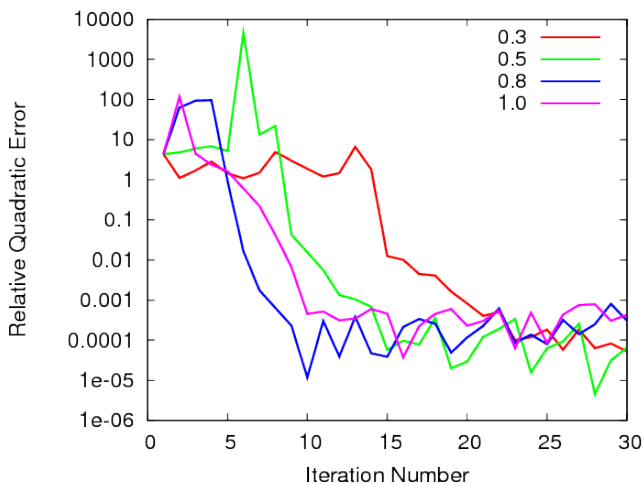


Figure 6. Effect of relaxation factor on convergence history. $\mu = 0.15$.

Akin to the investigation presented for $\mu = 0.3$, first

results concerning the effects of the relaxation parameter on the solution convergence history are presented in Fig. 6. It shows that also in this case the error decay is sped up when higher values of the relaxation factor (close to 1) are used. In the overall, the convergence error threshold tends to be reached more slowly with respect to the case with $\mu = 0.3$. Although not shown here, the analysis on the effect of aerodynamic Jacobian determined from different aerodynamics confirms that solution convergence is achieved neither when no Jacobian is included in the iterative process, nor when a quasi-steady solver is used.

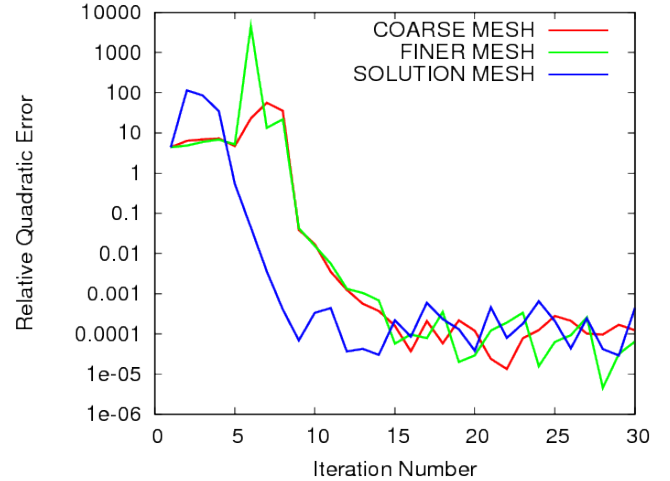


Figure 7. Effect of BEM mesh used for Jacobian evaluation on convergence history. $\mu = 0.15$.

Figure 7 presents the effect of the accuracy of the BEM solver used to determine the Jacobian on the aeroelastic convergence. For the present advance ratio the faster solution is clearly obtained using the finest ‘Solution’ mesh. However, the trade-off between convergence speed and computational costs would suggest the use of the coarse mesh.

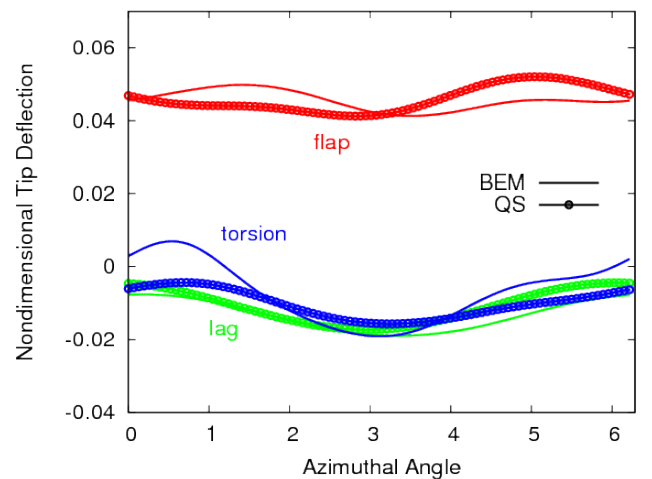


Figure 8. Blade tip deflections. $\mu = 0.15$.

The aeroelastic response results, given in terms of blade-tip deflections and vibratory hub loads, are presented in Figs. 8 and 9. The observation of the tip deflections reveals that, differently from what examined at $\mu = 0.3$, a phase shift of about 180° exists between the flap time history predicted by the BEM approach and that given

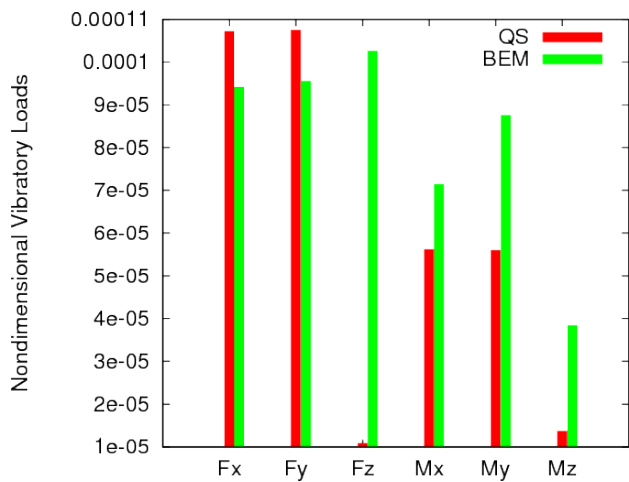


Figure 9. 4/rev vibratory hub loads. $\mu = 0.15$.

by quasi-steady aerodynamics, while two amplitudes are in agreement. Akin to what observed at $\mu = 0.3$, a higher harmonic content on the torsion deformation is present in the simulation from the BEM aerodynamics. In the overall, BEM and quasi-steady aerodynamics blade tip predictions are closer for $\mu = 0.15$ rather than for $\mu = 0.30$. Concerning the 4/rev vibratory hub loads, in this case the differences between quasi-steady and BEM aerodynamics predictions are significantly greater than those calculated at $\mu = 0.3$. This result is particularly evident for the out-of-plane load components. Note that the vibratory loads at low speed are about one order of magnitude smaller than those at $\mu = 0.30$, and this fact could be one important reason for the slower convergence rate observed.

CONCLUSIONS

A fully-coupled aeroelastic solver for the analysis of rotorcraft in steady flight conditions has been presented. Structural dynamics is based upon a non-linear beam model, while a BEM solver for potential flows is used for the evaluation of the airloads. The numerical space integration is performed through the Galerkin approach, while the time solution is evaluated by harmonic-balance technique. Performance and robustness of the proposed numerical solution algorithm has been analysed for a four-bladed rotor moving at two advance ratios. Particular attention has been paid on the effect of relaxation and Jacobian fidelity on the convergence rate of the solution. When using Jacobian numerically evaluated through the BEM solver, the convergence rate has shown to be satisfactory, however depending on the relaxation factor applied and the accuracy of BEM solver for Jacobian identification. No convergence is achieved if the aerodynamic Jacobian is evaluated by a simpler aerodynamic solver (a quasi-steady model has been considered in this work) or is even neglected. It has been shown that a coarse BEM mesh yields a Jacobian that guarantees quite fast convergence of the aeroelastic iteration process, at much lower computational costs.

Finally, the aeroelastic responses (in terms of blade tip displacements and vibratory hub loads) obtained by the proposed fully coupled aeroelastic solver have been com-

pared with those from quasi-steady aerodynamics. Major differences have been observed on the prediction of torsion deflection and out-of-plane vibratory loads.

ACKNOWLEDGMENTS

This work has been partially supported by the European Union Project ARISTOTEL (Grant agreement N. 266073), financed under the Seventh Framework Programme (FP7/2007-2013).

REFERENCES

- Gennaretti, M., Bernardini, G., 'Aeroelastic Response of Helicopter Rotors Using a 3-D Unsteady Aerodynamic Solver,' *The Aeronautical Journal*, Vol. 110, No. 1114, 2006, pp. 793-801.
- Gennaretti, M., Bernardini, G., 'Novel Boundary Integral Formulation for Blade-Vortex Interaction Aerodynamics of Helicopter Rotors,' *AIAA Journal*, Vol. 45, No. 6, 2007, pp. 1169-1176.
- Morino, L., 'A General Theory of unsteady compressible potential aerodynamics,' NASA CR-2464, 1974.
- Hodges, D.H., Dowell, E.H., 'Nonlinear Equation for the Elastic Bending and Torsion of Twisted nonuniform Rotor Blades,' NASA TN D-7818, December 1974.
- Hodges, D.H., Ormiston, R.A., 'Stability of Elastic Bending and Torsion of Uniform Cantilever Rotor Blades in Hover with Variable Structural Coupling,' NASA TN D-8192, April 1976.
- Gennaretti, M., Molica Colella, M., Bernardini, G., 'Prediction of Tiltrotor Vibratory Loads with Inclusion of Wing-Proprotor Aerodynamic Interaction,' *J. of Aircraft*, Vol. 47, No. 1, 2010, pp. 71-79.
- Morino, L., Gennaretti, M., 'Boundary Integral Equation Methods for Aerodynamics,' *Computational Nonlinear Mechanics in Aerospace Engineering*, edited by S.N. Atluri, Vol. 146, Progress in Astronautics & Aeronautics, AIAA, New York, 1992, pp. 279-320.
- Greenberg, J.M., 'Airfoil in sinusoidal motion in a pulsating stream,' NACA TN-1326, 1947.
- Theodorsen, T., 'General theory of aerodynamic instability and the mechanism of flutter,' NACA Report 496, 1935.
- van der Wall, B., Leishman, J.G., 'The Influence of Variable Flow Velocity on Unsteady Airfoil Behavior,' *J. of American Helicopter Society*, Vol. 39, No. 4, 1994, pp. 288-297.
- Bi, N.-P., Leishman, J.G., Crouse, G.L., 'Investigation of Rotor Tip Vortex Interactions with a Body,' *J. of Aircraft*, Vol. 30, No. 6, 1993, pp. 879-889.
- Zhang, J. Active-passive hybrid optimization of rotor blades with trailing edge flaps, PhD Thesis, Department of Aerospace Engineering, The Pennsylvania State University, 2001.

APPENDIX A

From the decomposition of the potential field into a scattered component, φ_s , and an incident component, φ_I (see section ‘Aerodynamic modelling’), in a body-fixed frame of reference the Bernoulli theorem reads

$$\dot{\varphi}_s + \dot{\varphi}_I - \mathbf{v}_B \cdot (\nabla\varphi_s + \mathbf{u}_I) + \frac{\|\nabla\varphi_s + \mathbf{u}_I\|^2}{2} + \frac{p}{\rho} = \frac{p_0}{\rho} \quad (11)$$

where p_0 is the pressure of the undisturbed medium. In order to evaluate the pressure distribution, the expression above requires the determination of $\dot{\varphi}_I$, which is the only term not directly available from the aerodynamic formulation presented in the section ‘Aerodynamic modelling’. The incident potential (and the corresponding time derivative) could be obtained from the doublet distribution over the far wake, S_w^F , using the following integral expression (see also Eq. (2))

$$\varphi_I(\mathbf{x}, t) = - \int_{S_w^F} \Delta\varphi_s(\mathbf{y}_w^{TE}, t - \vartheta) \frac{\partial G}{\partial n} dS(\mathbf{y}) \quad (12)$$

that, dividing the wake into panels, $S_{w_k}^F$, is approximated as

$$\varphi_I(\mathbf{x}, t) \approx - \sum_{k=1}^N -\Delta\varphi_s(\mathbf{y}_{w_k}^{TE}, t - \vartheta_k) \int_{S_{w_k}^F} \frac{\partial G}{\partial n} dS(\mathbf{y}) \quad (13)$$

However, as already mentioned in section ‘Aerodynamic modelling’, the above expression cannot be applied to those wake panels coming in contact with the body or passing very close to it (BVI occurrence), in that they become numerically unstable and yield unrealistic potential distributions.

In order to avoid this problem, for the far wake panels that might experience BVI, the contribution to $\dot{\varphi}_I$ is obtained in the following robust and accurate way. Consider the closed vortex at the contour of the k -th panel of the far wake that might risk to come in contact with the body, $C_k = \partial S_{w_k}^F$, and introduce a frame of reference rigidly connected with it such that, under the assumption of undeformed wake panel, the incident potential induced by the vortex is constant in time on each point of it. Next consider a body surface point and a vortex frame point that at a given time coincide. Observing that for a generic function, $f = f(\mathbf{x}, t)$,

$$\left. \frac{\partial f}{\partial t} \right|_V = \left. \frac{\partial f}{\partial t} \right|_B + \mathbf{v}_{B-V} \cdot \nabla f$$

where $\partial f/\partial t|_V$ and $\partial f/\partial t|_B$ denote time derivative observed, respectively, in the vortex frame and in the body frame, while $\mathbf{v}_{B-V} = \mathbf{v}_V - \mathbf{v}_B$ is the relative velocity between the two frames at the considered point, for $f = \varphi_I^k$ (with φ_I^k denoting the incident potential due to the k -th far wake vortex) and reminding that $\dot{\varphi}_I^k = 0$ in the vortex frame, it is possible to obtain for the time derivative of the incident potential in the body frame

$$\left. \frac{\partial \varphi_I^k}{\partial t} \right|_B = -\mathbf{v}_{B-V} \cdot \mathbf{u}_I^k \quad (14)$$

with \mathbf{u}_I^k known from the (regularized) k -th contribution in Eq. (3).

If the evaluation of the pressure is carried out within a free-wake solution, each far wake vortex is subject to deformation. In this case, the related (doublet) potential induced in the corresponding vortex frame is no longer stationary, although the intensity of the doublet is time independent (indeed, it is given by the potential jump across the wake that is constant following a material point [3, 7]). Nevertheless, this contribution is not taken into account for the vortices that are close to the evaluation point, in that negligible with respect to the contribution from the term in Eq. (14), due to the very high induced velocity arising.

A procedure similar to that described above for the evaluation of the $\dot{\varphi}_I^k$ from a wake vortex has been applied in Ref. [11] for the evaluation of the pressure on a body induced by vortex filaments.